

CROSSROADS IN EARTH AND PLANETARY MATERIALS

Crystal structures of laihunite and intermediate phases between laihunite-1M and fayalite: Z-contrast imaging and ab initio study

HUIFANG XU^{1,*}, ZHIZHANG SHEN¹, HIROMI KONISHI¹, PINGQIU FU² AND IZABELA SZLUFARSKA³

¹NASA Astrobiology Institute, Department of Geoscience, University of Wisconsin-Madison, Madison, Wisconsin 53706, U.S.A.

²Institute of Geochemistry, The Chinese Academy of Sciences, Guiyang, Guizhou 550002, P.R. China

³Department of Materials Science and Engineering, University of Wisconsin-Madison, Madison, Wisconsin 53706, U.S.A.

ABSTRACT

Crystals of laihunite from Xiaolaihe of Liaoning Province, northeast China, were studied using selected-area electron diffraction (SAED), high-resolution transmission electron microscopy (HRTEM), and Z-contrast imaging. Z-contrast images directly reveal ordered vacancies in M1 sites. The results confirm early structural models for 1-layer laihunite (or laihunite-1M) with ideal stoichiometry of $\square_{0.5}\text{Fe}_{0.5}^{2+}\text{Fe}^{3+}\text{SiO}_4$. 2-layer laihunite and 3-layer laihunite are found to be chemically different from laihunite-1M. The 2-layer laihunite can be viewed as a periodic intergrowth of laihunite and fayalite in the 1:1 ratio. The 3-layer laihunite can be considered to be a periodic intergrowth of laihunite and fayalite in the 1:0.5 ratio along the *c*-axis. Ideal stoichiometries for the 2-layer structure and the 3-layer structure are $\square_{0.5}\text{Fe}_{2.5}^{2+}\text{Fe}^{3+}[\text{SiO}_4]_2$ and $\square_{1.0}\text{Fe}_{3.0}^{2+}\text{Fe}_{2.0}^{3+}[\text{SiO}_4]_3$, respectively. The structural intergrowth of the 3-layer laihunite and the 1-layer laihunite results in chemical compositions falling within the range between the two aforementioned structures, such as the chemical formula of $\square_{0.4}\text{Fe}_{0.8}^{2+}\text{Fe}_{0.8}^{3+}\text{SiO}_4$, reported earlier in the literature.

The crystal structures of the 1-layer laihunite (1M), the 2-layer laihunite (2M), and the 3-layer laihunite (3Or) determined from Z-contrast images and ab initio calculations using the density functional theory (DFT) have space groups of *P2₁/b*, *P2₁/b*, and *Pbnm*, respectively. The previously reported monoclinic symmetry for the 3-layer laihunite may be an artifact due to overlapping diffraction spots from both, the laihunite-3Or and the laihunite-1M. Our study demonstrates that the method of combining Z-contrast imaging and ab initio calculation can be effectively used for identifying structures of nano-phases in host crystals. Perhaps more importantly, Z-contrast imaging provides a powerful means for direct observation of vacancies and other defects, and may be utilized to map vacancies in Fe³⁺-bearing olivines, the alignments of which can greatly affect anisotropic diffusion in such structures.

Keywords: Laihunite, vacancy ordering, Z-contrast imaging, DFT, HRTEM, superstructure, olivine, oxidation

INTRODUCTION

Laihunite that has a distorted olivine-type structure with ferric and ferrous irons and ordered distribution of vacancies was first discovered in a high-grade metamorphosed banded iron formation (BIF) (Laihunite Research Group 1976; Fu et al. 1982). The occurrence of laihunite is not limited to metamorphosed BIFs. Laihunite was also found in certain black fayalite (Schaefer 1983, 1985), martian meteorite (Noguchi et al. 2009), some ferric-fayalite from granite, and Fe-bearing olivine from volcanic and intrusive rocks (Sueno et al. 1985; Banfield et al. 1990, 1992; Janney and Banfield 1998; Putnis 1979; Xu et al. 1992; Konishi and Xu 2012). The laihunite, which coexists with fayalite, magnetite, quartz, ferrosilite, almandine, and hedenbergite, was formed in the process of oxidation of fayalite during metamorphism (Fu et al. 1982; Wang 1982; Kitamura et al. 1984). The structure refinement of the 1-layer laihunite shows *P2₁/b* symmetry and ordered arrangement of vacancies

in half of the M₁ sites of a fayalite structure (Fu et al. 1982). A proposed ideal structural formula for the 1-layer laihunite is $\square_{0.5}\text{Fe}_{0.5}^{2+}\text{Fe}^{3+}\text{SiO}_4$ (Fu et al. 1982). However, structural details regarding symmetry and the number of vacancies in the structures are still a matter of controversy (Fu et al. 1982; Tamada et al. 1983; Ferrifayalite Research Group 1976). To address these questions, it was proposed that the 1-layer structure is an average of the 3-layer laihunite that has a tripled periodicity along the *c*-axis with respect to fayalite structure (Shen et al. 1984; Tamada et al. 1983). A recent ab initio calculation result even suggested that 1-layer laihunite structure may have a triclinic symmetry (Chatterjee and Saha-Dasgupta 2010).

Transmission electron microscopy (TEM) and some X-ray studies have shown that there are also domains of fayalite, the 3-layer, and the 2-layer structures that are intergrown with laihunite (Li et al. 1981; Fu et al. 1982; Kitamura et al. 1984; Sueno et al. 1985; Chou 1985; Kondoh et al. 1985). Single-crystal structure refinement of a 3-layer laihunite was carried out based on *P2₁/b* symmetry (Shen et al. 1982, 1984). It was found that a 3-layer laihunite synthesized by oxidizing fayalite

* E-mail: hfxu@geology.wisc.edu

at high temperature has a higher Fe content than natural 2-layer and 3-layer laihunite structures do (Kondoh et al. 1985). At the same time, the synthetic 3-layer structure is different from the natural 3-layer laihunite in composition (Kondoh et al. 1985). All the reported TEM data suggest intergrowth of the laihunite structures at nanometer and sub-micrometer scales (1-layer, 2-layer, and 3-layer domains). Proposed models for the 3-layer laihunite superstructure are also controversial regarding the number of vacancies and the distributions of vacancies (Li et al. 1981; Shen et al. 1984; Chou 1985). A 3-layer laihunite structure with monoclinic symmetry determined using X-ray single-crystal diffraction method was proposed based on observation of overlapping diffraction peaks from multiple phases with the average composition of $\square_{0.4}\text{Fe}_{0.8}^{2+}\text{Fe}_{0.8}^{3+}\text{SiO}_4$ (Shen et al. 1984). In this paper, we use state-of-the-art methods of high-resolution Z-contrast imaging, in situ X-ray EDS analyses, and ab initio calculation based on the density functional theory (DFT) method to provide both structures and compositions of the laihunite (lahunite-1M) and intermediate phases between laihunite-1M and fayalite.

SAMPLE AND EXPERIMENT

Samples for TEM and associate X-ray energy-dispersive spectroscopy (EDS) investigation of laihunite crystals were obtained from Xiaolaihe, Liaoning Province, NE China, where in fact the laihunite was first discovered. The host rock of the above minerals is Archean metamorphosed BIF. Other coexisting minerals are fayalite, laihunite, magnetite, quartz, ferrosilite, and hedenbergite (Laihunite Research Group 1976; Ferrifayalite Research Group 1976).

Our first TEM experiments were carried out with a Philips 420ST electron microscope equipped with an EDAX energy-dispersive X-ray spectrometer and

a Princeton Gamma-Tech System-4000 analyzer as that described by Livi and Veblen (1987). Transmission electron microscopy and scanning transmission electron microscopy (STEM) studies were carried out using a FEI Titan 80-200 aberration corrected scanning/transmission electron microscope operated at 200 kV coupled with an EDAX high-resolution EDS detector and Gatan image filtering system. This instrument is capable of imaging single atoms with ~ 0.1 nm spatial resolution in STEM mode. Probe current was set at 24.5 pA. Collection angle of HAADF detector for acquiring all the Z-contrast images ranges from 54 to 270 mrad [corresponding to 7.5 ($1/\text{\AA}$) to 38.2 ($1/\text{\AA}$) in reciprocal space].

The scanning transmission electron microscopy (STEM) method uses the high-angle annular dark-field (HAADF) detector to give the most highly localized 1s Bloch state imaging, which eliminates most of the obvious effects of dynamical diffraction. Z-contrast images are HAADF images with atomic resolution (Kirkland 1998). The intensity of Z-contrast images depends on numbers of atoms (n) in an atomic column (or occupancy) and atomic number of atoms in the sites through $\sim Z^2$ (Pennycook 2002). Local composition and occupancy may be obtained from measured intensities. The relationship between intensity and atomic number for the experimental condition based on calculated intensities for atoms columns in a Co-Mn-Si alloy is $\sim Z^{2.27}$ (Shi 2013).

Specimens for TEM/STEM investigation were prepared by crushing the selected crystals in alcohol and then depositing a drop of crystal suspension on holey-carbon Cu-grids. Because of fairly well-developed {100} and {010} cleavages of fayalite and laihunite, it is not difficult to get crystal grains containing 00/ diffraction in their diffraction patterns. Fayalite (Fe_2SiO_4) and forsterite (Mg_2SiO_4) were used as a standard for determination of the K-factor of Fe and Mg. All settings for the X-ray energy-dispersion spectra (EDS) collections were the same as for the K-factor determination. Fe^{2+} and Fe^{3+} of the laihunite were calculated from the $(\text{Fe}+\text{Mg}+\text{Mn}+\text{Ca}+\text{Ni})/\text{Si}$ ratio deduced from the EDS results, by considering charge balance and assuming all tetrahedral sites are occupied by Si. X-ray EDS analysis from a small area with known structure can be obtained by combining selected-area electron diffraction (SAED) and HRTEM images collected from the same area. This analysis is possible because SAED and HRTEM can provide structural information from very small areas, such as domains of 1-layer laihunite,

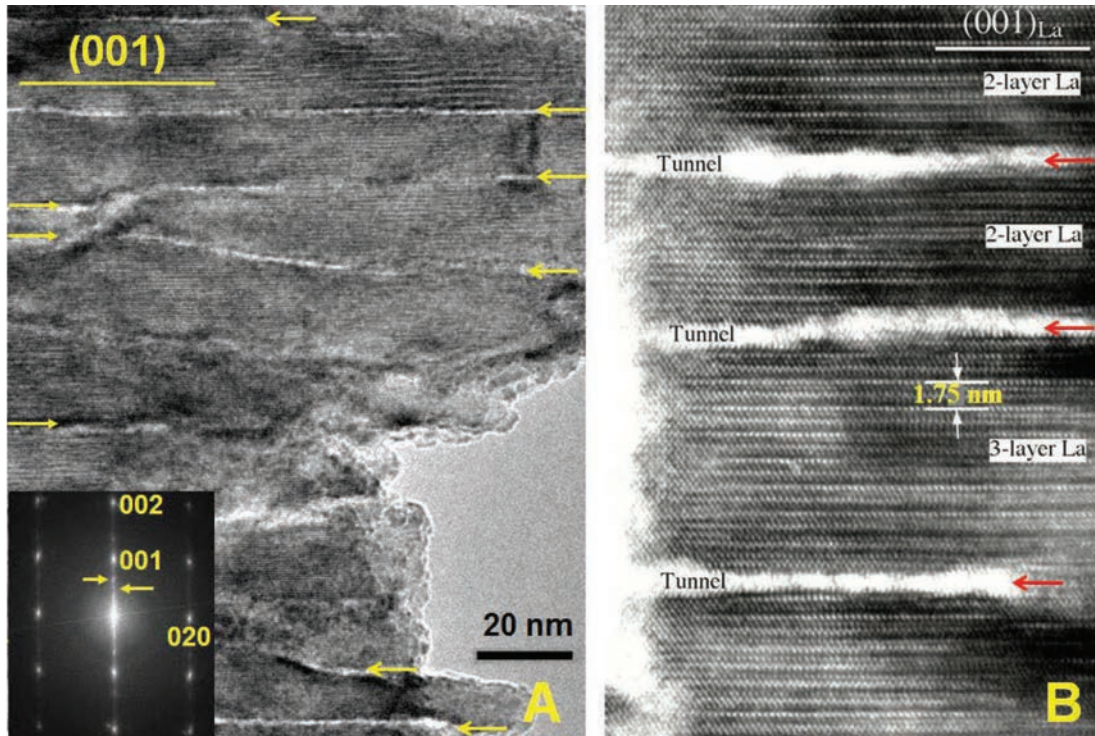


FIGURE 1. (a) TEM image showing a structural heterogeneity of a laihunite crystal with nano-cracks or nano-tunnels (indicated by arrows) between neighboring domains. Nano-cracks formed during the transformation from fayalite to laihunite due to the difference in the c -dimensions between fayalite and laihunite. Inserted FFT pattern shows streaking along the c^* direction and intensity maxima at $00 \frac{1}{2}$ and $00 \frac{3}{2}$ positions (indicated by 2 short arrows). (b) An HRTEM image showing intergrowth of 2-layer and 3-layer laihunite domains and nano-tunnels.

2-layer laihunite, and 3-layer laihunite.

The DFT calculations were performed by using Vienna Ab initio Simulation Package (VASP) (Kresse and Furthmüller 1996). The general gradient approximation (GGA) with the Perdew, Burke, and Ernzerhof (PBE) parameters was employed (Perdew et al. 1996). The projector-augmented wave (PAW) method with the energy cutoff of 600 eV was used. K-point meshes of $4 \times 4 \times 2$, $4 \times 2 \times 2$, and $4 \times 1 \times 2$ were found to be sufficient for 1-layer, 2-layer, and 3-layer laihunite structures, respectively. To take into account the on-site Coulomb repulsion of 3d electron in Fe atoms, we employed a simplified (rotationally invariant) approach known as GGA+U (Dudarev et al. 1998). In Dudarev's method, an effective U parameter, $U_{\text{eff}} = U - J$, is used. According to previous DFT calculations of fayalite (Cococcioni et al. 2003; Stackhouse et al. 2010), $U_{\text{eff}} = 4.8$ eV is a reasonable value and thus it was used in this study. All initial structures with $P1$ symmetry proposed in this study were relaxed using the static energy minimization scheme, where both the shape and volume of the cell were allowed to relax. The final structures with lowest energy states are chosen as possible structures for the three phases. The electron diffraction patterns of calculated structures were generated by SingleCrystal software.

RESULTS AND DISCUSSION

TEM results

TEM images show that the crystals are heterogeneous in structure with nano-cracks between neighboring domains (Fig. 1). Selected-area electron diffraction (SAED) patterns show that the crystal contains laihunite (or 1-layer laihunite), 3-layer laihunite domains, 2-layer laihunite domains, and fayalite domains (Fig. 2). We found many areas with intergrown 3-layer and 1-layer laihunite structures (Figs. 2d and 2e). The SAED pattern (Fig. 2e) shows diffractions from 1-layer laihunite and 3-layer laihunite. Positions of 001 and 003 are not from the 3-layer laihunite domain, but from 1-layer laihunite domain, because they are off the center between $00 \frac{1}{3}$ and $00 \frac{2}{3}$,

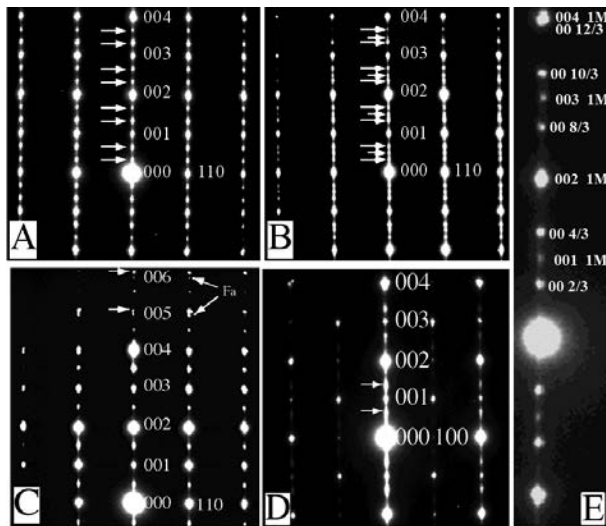


FIGURE 2. SAED patterns from 3-layer laihunite (a), intergrown 2-layer and 3-layer laihunite (b), intergrown fayalite and 2-layer laihunite (c), [010]-zone axis of intergrown 1-layer and 2-layer laihunite (d), and tilted crystal with only 00l reflections to avoid multiple diffraction from hkl spots (e). All the indices are based on fayalite unit-cell setting. Arrows in (a) indicate extra spots from tripled periodicity along the c -axis. Long arrows and short arrows in (b) indicate diffraction spots from 3-layer and 2-layer laihunite, respectively. SAED (c) shows splitting in high-order 00l reflections (005, 006) from fayalite and the 2-layer laihunite domain. All the indices are based on fayalite setting.

TABLE 1. Unit-cell parameters of 1-layer, 2-layer, and 3-layer laihunite structures

	Experiment (Å)	DFT calculations (Å)
Laihunite-1M	4.80, 10.20, 1×5.80	4.808, 10.230, 1×5.808
Laihunite-3Or	4.81, 10.25, 3×5.85	4.824, 10.291, 3×5.882
Laihunite-2M	4.82, 10.30, 2×5.93	4.826, 10.319, 2×5.931
Fayalite	4.8195, 10.4788, 6.0873	4.8304, 10.4359, 6.0852

Notes: The experimental values are measured from electron diffraction and FFT patterns. Values for fayalite are from Fujino et al. (1981). Uncertainty for the measured unit-cell parameters is about ± 0.02 Å.

TABLE 2. Structural formulas for fayalite and laihunite domains

Structural formula	Analyzed domain
$(\square_{0.00}\text{Fe}_{0.93}^{2+}\text{Mg}_{0.05}\text{Mn}_{0.01}\text{Ca}_{0.00}\text{Ni}_{0.01})\text{SiO}_4$	fayalite
$(\square_{0.21}\text{Fe}_{1.28}^{2+}\text{Fe}_{0.42}^{3+}\text{Mg}_{0.07}\text{Mn}_{0.00}\text{Ca}_{0.01}\text{Ni}_{0.01})\text{SiO}_4$	2-layer laihunite
$(\square_{0.21}\text{Fe}_{1.28}^{2+}\text{Fe}_{0.43}^{3+}\text{Mg}_{0.06}\text{Mn}_{0.01}\text{Ca}_{0.00}\text{Ni}_{0.01})\text{SiO}_4$	2-layer laihunite
$(\square_{0.25}\text{Fe}_{1.25}^{2+}\text{Fe}_{0.44}^{3+}\text{Mg}_{0.05}\text{Mn}_{0.00}\text{Ca}_{0.01}\text{Ni}_{0.00})\text{SiO}_4$	2-layer laihunite
$(\square_{0.225}\text{Fe}_{1.1}^{2+}\text{Fe}_{0.35}^{3+}\text{Mg}_{0.06}\text{Mn}_{0.01}\text{Ca}_{0.00}\text{Ni}_{0.00})\text{SiO}_4$	2-layer laihunite
$(\square_{0.25}\text{Fe}_{1.15}^{2+}\text{Fe}_{0.50}^{3+}\text{Mg}_{0.09}\text{Mn}_{0.00}\text{Ca}_{0.00}\text{Ni}_{0.01})\text{SiO}_4$	2-layer laihunite
$(\square_{0.25}\text{Fe}_{1.16}^{2+}\text{Fe}_{0.39}^{3+}\text{Mg}_{0.09}\text{Mn}_{0.01}\text{Ca}_{0.00}\text{Ni}_{0.01})\text{SiO}_4$	2-layer laihunite
$(\square_{0.30}\text{Fe}_{1.00}^{2+}\text{Fe}_{0.60}^{3+}\text{Mg}_{0.08}\text{Mn}_{0.01}\text{Ca}_{0.01}\text{Ni}_{0.00})\text{SiO}_4$	3-layer laihunite
$(\square_{0.33}\text{Fe}_{0.91}^{2+}\text{Fe}_{0.66}^{3+}\text{Mg}_{0.08}\text{Mn}_{0.01}\text{Ca}_{0.01}\text{Ni}_{0.00})\text{SiO}_4$	3-layer laihunite
$(\square_{0.34}\text{Fe}_{0.85}^{2+}\text{Fe}_{0.67}^{3+}\text{Mg}_{0.06}\text{Mn}_{0.00}\text{Ca}_{0.00}\text{Ni}_{0.01})\text{SiO}_4$	3-layer laihunite
$(\square_{0.35}\text{Fe}_{0.84}^{2+}\text{Fe}_{0.70}^{3+}\text{Mg}_{0.10}\text{Mn}_{0.00}\text{Ca}_{0.00}\text{Ni}_{0.01})\text{SiO}_4$	3-layer laihunite
$(\square_{0.35}\text{Fe}_{0.88}^{2+}\text{Fe}_{0.69}^{3+}\text{Mg}_{0.06}\text{Mn}_{0.01}\text{Ca}_{0.00}\text{Ni}_{0.01})\text{SiO}_4$	3-layer laihunite
$(\square_{0.37}\text{Fe}_{0.82}^{2+}\text{Fe}_{0.74}^{3+}\text{Mg}_{0.07}\text{Mn}_{0.00}\text{Ca}_{0.00}\text{Ni}_{0.00})\text{SiO}_4$	3-layer laihunite
$(\square_{0.39}\text{Fe}_{0.75}^{2+}\text{Fe}_{0.77}^{3+}\text{Mg}_{0.07}\text{Mn}_{0.01}\text{Ca}_{0.01}\text{Ni}_{0.01})\text{SiO}_4$	3-layer laihunite
$(\square_{0.47}\text{Fe}_{0.50}^{2+}\text{Fe}_{0.95}^{3+}\text{Mg}_{0.08}\text{Mn}_{0.00}\text{Ca}_{0.00}\text{Ni}_{0.00})\text{SiO}_4$	1-layer laihunite
$(\square_{0.48}\text{Fe}_{0.48}^{2+}\text{Fe}_{0.95}^{3+}\text{Mg}_{0.08}\text{Mn}_{0.00}\text{Ca}_{0.00}\text{Ni}_{0.00})\text{SiO}_4$	1-layer laihunite
$(\square_{0.49}\text{Fe}_{0.49}^{2+}\text{Fe}_{0.98}^{3+}\text{Mg}_{0.04}\text{Mn}_{0.00}\text{Ca}_{0.00}\text{Ni}_{0.00})\text{SiO}_4$	1-layer laihunite
$(\square_{0.51}\text{Fe}_{0.38}^{2+}\text{Fe}_{1.02}^{3+}\text{Mg}_{0.09}\text{Mn}_{0.00}\text{Ca}_{0.00}\text{Ni}_{0.00})\text{SiO}_4$	1-layer laihunite
$(\square_{0.52}\text{Fe}_{0.36}^{2+}\text{Fe}_{1.04}^{3+}\text{Mg}_{0.07}\text{Mn}_{0.00}\text{Ca}_{0.00}\text{Ni}_{0.00})\text{SiO}_4$	1-layer laihunite
$(\square_{0.52}\text{Fe}_{0.36}^{2+}\text{Fe}_{1.04}^{3+}\text{Mg}_{0.08}\text{Mn}_{0.00}\text{Ca}_{0.00}\text{Ni}_{0.00})\text{SiO}_4$	1-layer laihunite

and $00 \frac{1}{3}$ reflections (fractional indices are based on fayalite unit cell and setting). Periodicity along the c -axis for the 3-layer laihunite is $1.5c$ of the 1-layer laihunite. Diffraction spots of 001 and 003 from a 1-layer laihunite should not be considered as 003 and 009 diffractions of the 3-layer laihunite structure. Unit-cell parameters can be measured by comparing the diffraction difference and fast Fourier transform (FFT) patterns between known structure (fayalite) and unknown laihunite phases with different periodicities along their c -axes (Table 1).

X-ray EDS spectra of laihunite with different structures (different periodicities along the c -axis) were collected from relatively ordered domains and confirmed by SAED patterns and HRTEM images. Using a general formula for laihunite $\square_x\text{Fe}_{2-3x}^{2+}\text{Fe}_{2x}^{3+}\text{SiO}_4$, we found the number of vacancies for the 1-layer laihunite range from 0.47–0.52; the amount of vacancies for the 3-layer laihunite range from 0.30–0.39; and the amount of vacancies for the 2-layer laihunite range from 0.21–0.25. The observed laihunite domains with difference periodicities are chemically distinct (Table 2), and they are not in simple substructure and superstructure relationships.

Z-contrast imaging results

Z-contrast image of a fayalite area shows the positions of Fe (bright spots) and Si (much less bright spots among 3 Fe atoms). A structure model of fayalite is also overlaid on the image. Positions of oxygen are omitted for clarity because scattering from oxygen atom is much weaker than those from Fe and Si atoms. The diffraction spots of 00l ($l = \text{odd}$) appear in SAED pattern (Fig. 2c) and FFT pattern (Fig. 3c) from fayalite due to multiple diffraction of coherent scattered electrons at low-angle. Z-contrast images that use the high-angle annular dark-field

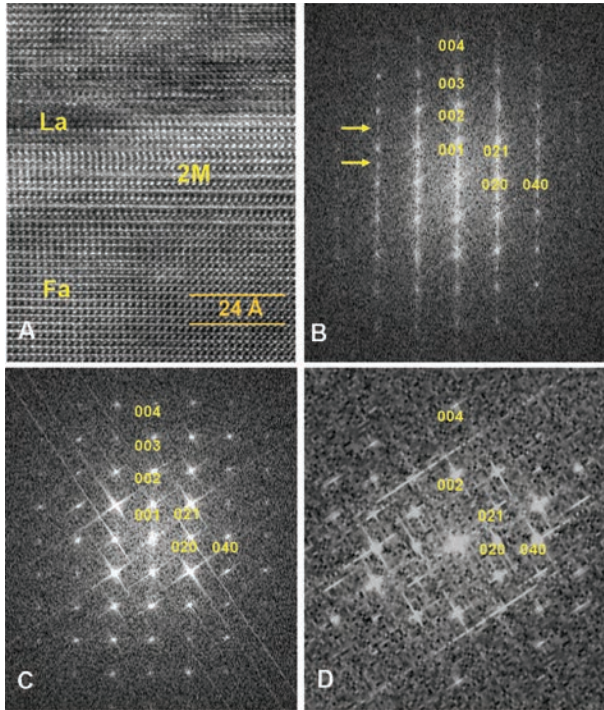


FIGURE 3. (a) [100]-zone-axis HRTEM image showing an interface between fayalite (Fa) and 2-layer laihunite (2M). FFT patterns from the 2M domain (b) and fayalite (c) areas show 001 and 003 spots that violate twofold screw axis due to the multiple diffraction effect in HRTEM imaging. The two arrows indicate spots from the 2-layer laihunite domain. It should be noted that the FFT pattern from the Z-contrast image of Figure 3 does not show 001 and 003 spots because Z-contrast image uses non-coherent scattered electrons at high angle and eliminates multiple diffraction effect (d).

(HAADF) detector to collect non-coherent scattered electrons at high angles eliminate most of the obvious effects of dynamical diffraction (Pennycook 2002). FFT pattern from the Z-contrast image of Figure 4 does not show 001, 003 spots due to twofold screw axis along the *c*-axis in fayalite structure (Fig. 4d).

A [100]-zone-axis Z-contrast image at the interface between fayalite and laihunite shows Fe vacancies at M1 sites within some of the (001) planes. Periodic distribution of the vacancies results in locally ordered domains of 2-layer laihunite (labeled 2) and 3-layer laihunite (labeled 1.5) (Fig. 5). A [110]-zone-axis Z-contrast image shows intergrowth of 1-layer laihunite, 2-layer laihunite, and 3-layer laihunite domains (Fig. 6). The Z-contrast images directly show positions of Fe vacancies in some of the M1 sites of fayalite-based structure. Structure models for 1-layer, 2-layer, and 3-layer laihunite can be obtained based on observed distribution of vacancies in fayalite-based structure. Figure 7 is a [100]-zone-axis Z-contrast image of 1-layer laihunite domain. Half of the M1 sites are vacancies in the 1-layer laihunite. Structure model for the 1-layer laihunite is also overlaid on the original image (Fig. 7a) and the noise-filtered image (Fig. 7b). The structure of the 1-layer laihunite is found to have a monoclinic symmetry. Some areas show a twin relationship between neighboring 1-layer laihunite domains and interface between 1-layer

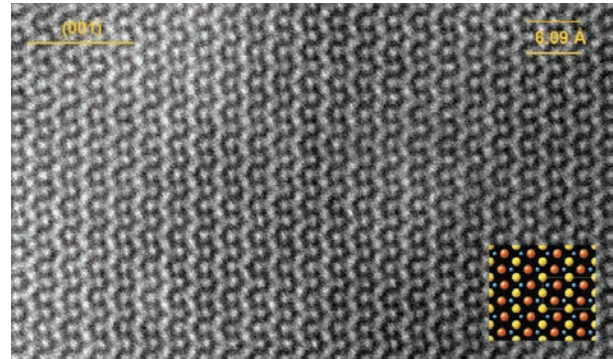


FIGURE 4. Z-contrast image of fayalite ([100]-zone axis) shows positions of Fe in M1 and M2 sites. Fayalite model is also overlaid on the image. Si atoms at the center among 3 Fe atoms (2 Fe at M1 site and one Fe in M2 site). Oxygen atoms are omitted because they are not visible in Z-contrast images due to the weak intensity with respect to Fe and Si. The Fe atoms at M1 and M2 sites, and Si atoms are colored in yellow, orange, and blue, respectively.



FIGURE 5. A [100]-zone-axis Z-contrast image showing interface between fayalite and laihunite domains with doubled (2) and tripled (1.5) periodicities along the *c*-axis.

and 3-layer laihunite (Fig. 8). Stoichiometry for the 1-layer laihunite domains is $\square_{0.5}\text{Fe}_{0.5}^{2+}\text{Fe}^{3+}\text{SiO}_4$ based on the number of vacancies in half of the M1 sites. Fe in M2 site neighboring the vacancies will be ferric Fe to maintain the local charge balance. This assertion is consistent with chemical compositions found

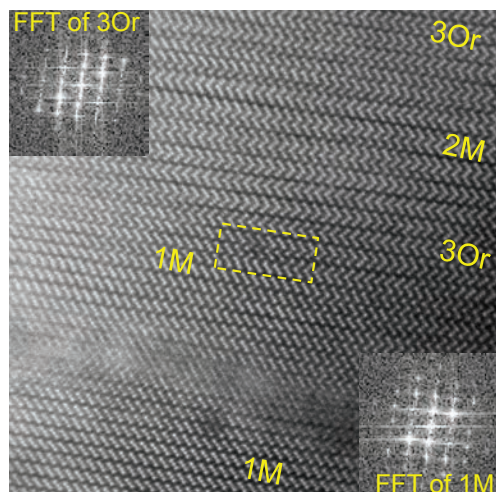


FIGURE 6. A [110]-zone-axis Z-contrast image showing intergrowth of 1-layer laihunite (1M), 2-layer laihunite (2M), and 3-layer laihunite (3Or). Inserted in the upper left and lower right corners are FFT patterns from 3-layer laihunite and 1-layer laihunite domains, respectively. An outline box area shows an interface between the 1-layer laihunite (1M) and the 3-layer laihunite (3Or).

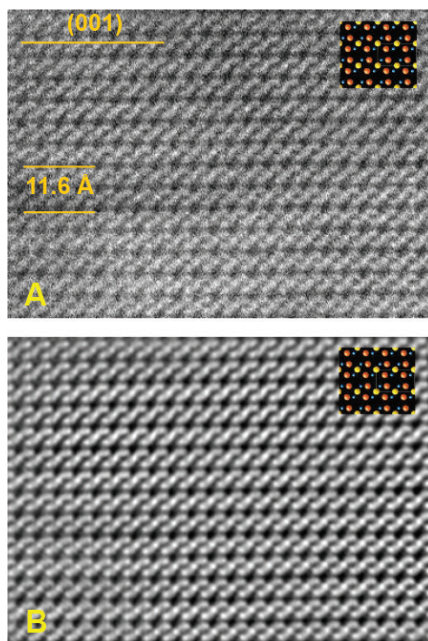


FIGURE 7. Z-contrast images of 1-layer laihunite ([100]-zone-axis) showing positions of high-density spots (corresponding to Fe, Si) and low-density sites of vacancies. Noise-filtered image (b) better shows the positions of the atoms and vacancy sites. A unit cell of 1-layer laihunite model with the $\square_{0.5}\text{Fe}_{0.5}^{2+}\text{Fe}^{3+}\text{SiO}_4$ stoichiometry is also overlaid on the image. The Fe atoms at M1 and M2 sites, and Si atoms are colored in yellow, orange, and blue, respectively.

by analyzing laihunite-1M domains (Table 2).

A [110]-zone-axis Z-contrast image from an area dominated by 3-layer laihunite shows that (001) vacancy layers occur every one and half fayalite units along the *c*-axis. Periodicity along the *c*-axis is tripled with respect to the fayalite structure (Fig. 9). FFT

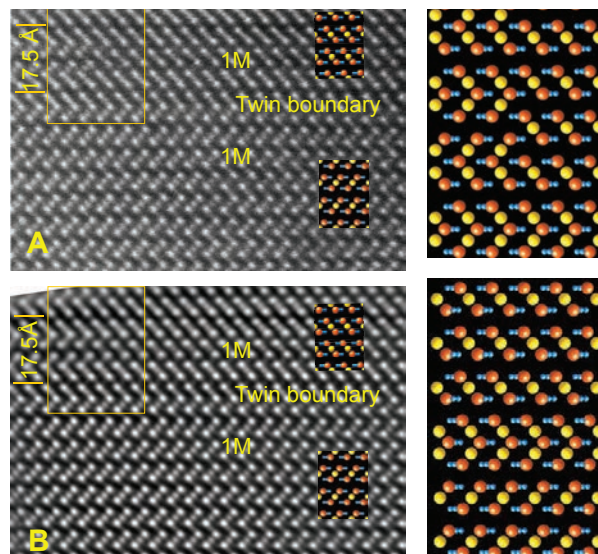


FIGURE 8. A [110]-zone-axis Z-contrast image of 1-layer laihunite (a raw image and a noise-filtered image) showing twinning relationship between the two neighboring 1-layer laihunite domains. M2 sites are brighter than M1 sites due to overlapping of Si and Fe^{3+} in the M2 sites along the [110] direction. It is also possible that a small number of Mg atoms migrated into M1 sites. The twin boundary (TB) is a unit cell of fayalite that was proposed by Fu et al. (1982). A unit cell of 1-layer laihunite model with the $\square_{0.5}\text{Fe}_{0.5}^{2+}\text{Fe}^{3+}\text{SiO}_4$ stoichiometry is also overlaid on the image. An outlined area in the upper left corner shows an interface between 1-layer laihunite and 3-layer laihunite. Models for the interface (upper) and twin relationship (lower) are shown on the right hand side of the images. The Fe atoms at M1 and M2 sites, and Si atoms are colored in yellow, orange, and blue, respectively.

pattern from the image shows 002 and 004 spots, which indicates a twofold screw axis along the *c*-axis of the 3-layer laihunite structure. The 3-layer laihunite will keep orthorhombic symmetry (or, laihunite-3Or). Stoichiometry for the laihunite-3Or will be $\square_{1.0}\text{Fe}_{3.0}^{2+}\text{Fe}_{2.0}^{3+}[\text{SiO}_4]_3$. This is consistent with chemical compositions from analyzed laihunite-3Or domains (Table 2). The structural intergrowth of 3-layer laihunite and 1-layer laihunite will result in chemical compositions that lie between the ideal 1-layer laihunite and 3-layer laihunite, such as the reported chemical formula of $\square_{0.4}\text{Fe}_{0.8}^{2+}\text{Fe}_{0.8}^{3+}\text{SiO}_4$ (Shen et al. 1984).

DFT calculations

Z-contrast images provide structure models that are based on compositions and distributions of vacancies among the M1 sites of fayalite-based structure. To obtain detailed atomic positions for the proposed structure models, we carried out *ab initio* calculation using DFT. In these calculations, it is important to consider magnetic properties of Fe in a given structure. According to published data, there are two possible antiferromagnetic (AF) configurations of fayalite: AF interaction between edge-sharing octahedra and AF interaction between corner-sharing octahedra (Cococcioni et al. 2003). In DFT calculations of 1-layer laihunite (Chatterjee and Saha-Dasgupta 2010), the latter configuration was found to have a lower energy. Our calculations confirm that the latter configuration is more stable for all three laihunite struc-

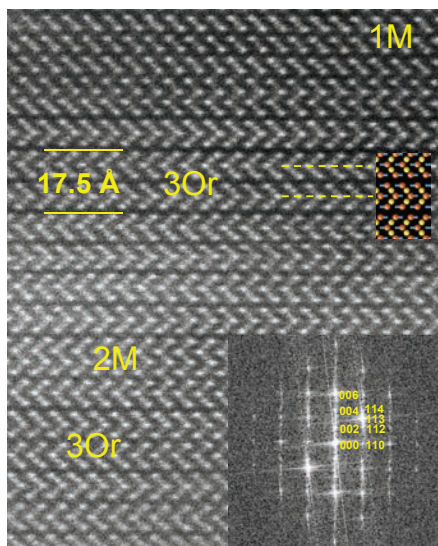


FIGURE 9. [110]-zone-axis Z-contrast image of an area dominated by 3-layer laihunite with domains of 1-layer laihunite (at top) and 2-layer laihunite. FFT pattern from the 3-layer laihunite shows even $00l$ spots ($l = 2n$, indexing is based on 3-layer laihunite setting). There are two vacancy layers per unit cell along (001). Ideal stoichiometry for the 3-layer laihunite is $\square_{1.0}\text{Fe}_{3.0}^2+\text{Fe}_{2.0}^3[\text{SiO}_4]_3$ that is two 1-layer laihunite units + one fayalite unit. Both the image and FFT pattern indicate that there is a twofold screw axis parallel to the c -axis, and two mirror planes parallel to (001) within one unit cell at the position of the dashed lines. A projection of 3-layer laihunite structure (Fe and Si atoms only) is also overlaid on the image.

tures (see appendix¹). Therefore, the laihunite structures reported below were calculated using the second magnetic configuration.

The distributions of vacancies in the initial structure models were based on the STEM observation that all vacancies occupy the M1 sites of fayalite-based structure. The optimized configurations with lowest energy for 1-layer, 2-layer, and 3-layer laihunite structures are shown in Figures 10 and 11. A monoclinic structure model (lahunite-3M) based on Shen et al. (1984) is also illustrated for comparison. Obviously, the “lahunite-3M” model does not fit observed Z-contrast images. The unit-cell parameters calculated from DFT are reported in Table 1 and they show a good agreement with the experimentally measured values. Because of the vacancy positions, the symmetries of 1-layer and 2-layer laihunite structures are reduced to monoclinic (the α angle are 91.39° and 90.79° , respectively), whereas 3-layer laihunite structure retains the orthorhombic symmetry. The 1-layer and 2-layer laihunite structures have space group $P2_1/b$ (no. 14) (Table 3). The 3-layer laihunite structure resumes the same space group of $Pbnm$ (no. 62) as fayalite (Table 3). Here, we use laihunite-1M, laihunite-2M, and laihunite-3Or to represent the observed 1-layer, 2-layer, and 3-layer laihunite structures, although they are not polymorphs with the same composition.

In laihunite-1M, the M1-O₆ octahedra are larger than the

M2-O₆ octahedra. In addition, the M2-O₆ octahedra are slightly more distorted (Table 4), which is consistent with conclusions from earlier calculations, although the earlier calculations suggest a triclinic symmetry for the 1-layer laihunite (Chatterjee and Saha-Dasgupta 2010). Comparing all the structure models with fayalite structure, the positions for Si and Fe2 are shifted away from their ideal positions in fayalite (fractional coordinate $z = 0.25$ for Si and Fe2), because of the presence of Fe(III) in those Fe2 sites that neighbor the vacancies (Table 5). However, fractional coordinates for Si and Fe2 in all the reported structures are different (Table 5). Our calculated structure shows that both Fe2 and Si atoms are slightly shifted toward vacancy sites, instead of opposite shifts along the c -axis with respect the Si and Fe positions in fayalite structure.

For laihunite-2M we find that, while there are similar M1-O₆ and M2-O₆ (Fe³⁺-O₆) octahedra adjacent to the vacancies as in laihunite-1M, the octahedra away from vacancies resemble those in fayalite. The laihunite-2M domains will also form twins, similarly to those observed in laihunite-1M.

In laihunite-3Or, there is just one type of M1-O₆ octahedra due to its orthorhombic symmetry (Table 4). The calculated laihunite-3Or structure is different from a previously proposed structure with monoclinic symmetry (Shen et al. 1984). The laihunite crystals contain nanometer to sub-micrometer scales of domains of all three laihunite structures and even residual fayalite. The crystal analyzed by Shen et al. (1984) contains domains of laihunite-1M and laihunite-3Or. X-ray diffraction peaks from the crystal will overlap with peaks from laihunite-1M and laihunite-3Or. If odd $00l$ reflections from laihunite-1M are considered as 003 and 009 reflections (based on 3-layer laihunite setting), the obtained structure will have a monoclinic symmetry ($P2_1/b$) instead of an orthorhombic symmetry ($Pbnm$). Structural intergrowth of 3-layer laihunite and 1-layer laihunite will result in average chemical compositions between the laihunite-1M and laihunite-3Or. The reported formula of $\square_{0.4}\text{Fe}_{0.8}^{2+}\text{Fe}_{0.8}^{3+}\text{SiO}_4$ (Shen et al. 1984) is an average composition of laihunite-1M and laihunite-3Or.

Chou (1985) proposed 2 types of 3-layer laihunite structures based on HRTEM images from [110]-zone-axis (for 3C1 structure odd and even $00l$ reflections) and [010]-zone axis (for 3C2

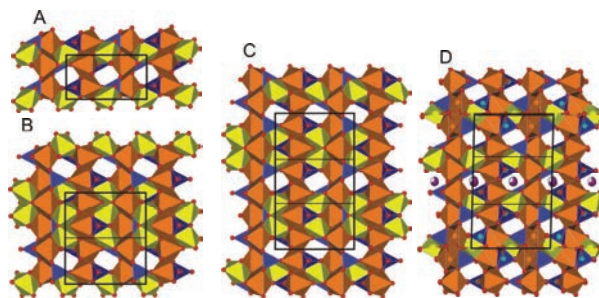


FIGURE 10. Polyhedral models along the a -axis projection for laihunite-1M (a), laihunite-2M (b), laihunite-3Or (c), and a previously proposed “lahunite-3M” (d) structure for the 3-layer laihunite. The “lahunite-3M” (d) is not a correct model, because it does not fit the observed Z-contrast images. The polyhedral for Fe atoms at M1 and M2 sites are colored in yellow and orange, respectively.

¹ Deposit item AM-14-509, Figures and Tables, CIF. Deposit items are stored on the MSA web site and available via the *American Mineralogist* Table of Contents. Find the article in the table of contents at GSW (ammin.geoscienceworld.org) or MSA (www.minsocam.org), and then click on the deposit link.

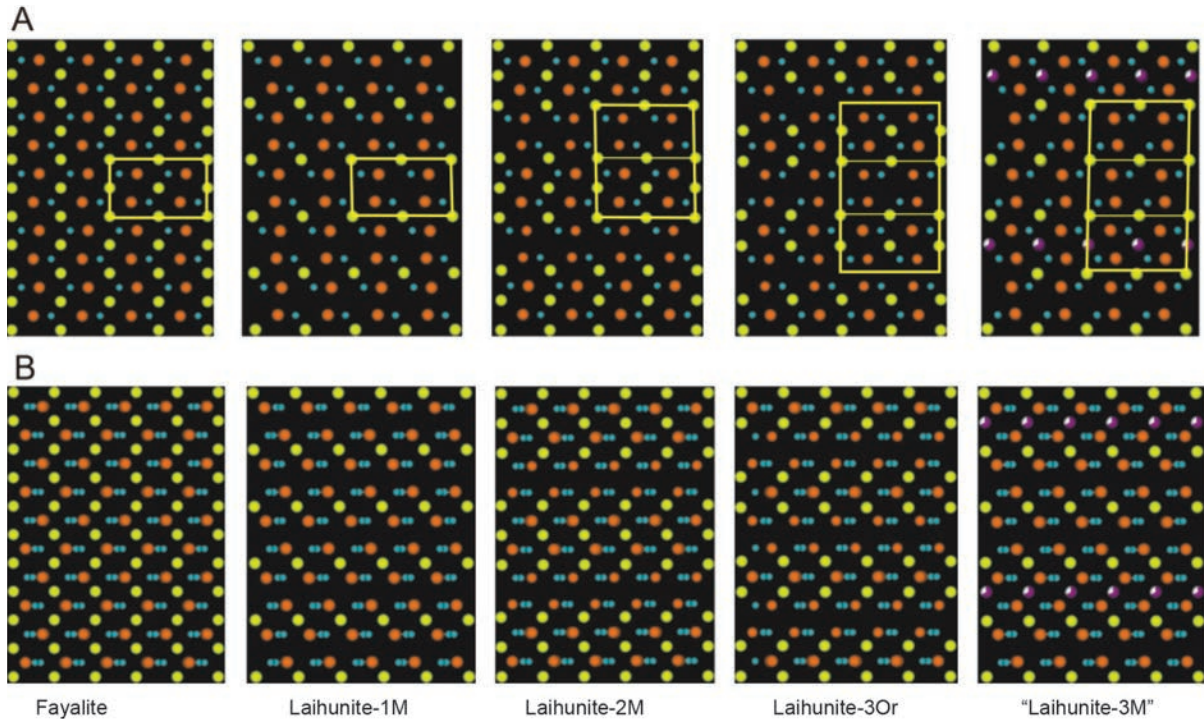


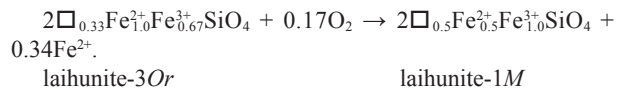
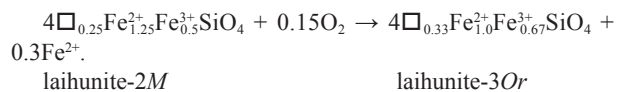
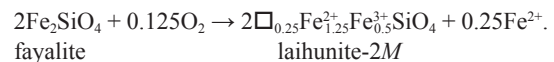
FIGURE 11. Projections of Fe and Si atoms of laihunite-1*M*, laihunite-2*M*, laihunite-3*Or*, and a previously proposed “laihunite-3*M*.” Panels (a) and (b) illustrate projections of the proposed structures along *a*-axis and [110]-zone axis, respectively. The Fe atoms at M1 and M2 sites, Si are colored in yellow, orange, and blue, respectively. The O atoms are omitted due to the weak intensity. Fe(III) in M2B sites neighboring vacancy sites are slightly smaller than Fe(II) in Fe2A sites to show the difference between them.

structure with even $00l$ reflections). According to our Z-contrast images and calculated structure (*Pbnm*) for the laihunite-3*Or*, odd $00l$ reflections and tripled periodicity along the *c*-axis in [110]-zone-axis SAED pattern and high-resolution transmission electron microscopic (HRTEM) images may be artifacts from multiple diffractions. In [010]-zone-axis SAED pattern and HRTEM image, there will be no odd $00l$ reflections due to *n*-glide plane perpendicular to (010). There is only one type of 3-layer structure, i.e., laihunite-3*Or*.

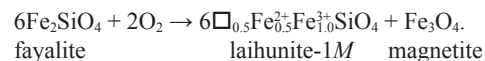
The observed 2-layer and 3-layer structures are not simple superstructures of laihunite-1*M*, because their compositions are different from that of laihunite-1*M*. The originally proposed laihunite structure has 1-layer periodicity with ideal stoichiometry of $\square_{0.5}\text{Fe}_{0.5}^{\text{II}}\text{Fe}^{\text{III}}\text{SiO}_4$ (Laihunite Research Group 1976; Fu et al. 1982). The observed intermediate phases are very similar to those in mixed-layer clay minerals, such as interstratified chlorite/serpentine minerals (Banfield and Bailey 1996; Xu and Veblen 1996). The observed intermediate structures in the laihunite-fayalite system and forsterite–Mg-laihunite system may be also described as interstratified olivine/laihunite minerals.

We propose that the observed laihunite structures are stable only within the fayalite host and we propose the following scenario for formation of these structures. Generally, the laihunite domains are formed during oxidative reaction of the fayalite in the solid state. Domains formed in early stage contain fewer vacancies and they serve as host phases to stabilize domains

formed at later stages and with more vacancies. The reactions for the laihunite formation may be simplified as



Extra Fe, generated as a product of the above reactions, diffuses out of the lattice and precipitates as magnetite at some tunnels areas (Figs. 1 and 12). Formation of laihunite results in shrinking of the unit cells, especially along the *c*-axis (Table 1) and in formation of nano-tunnels or cracks that parallel to (001). The net reaction for the laihunite formation of fayalite can be written as



The migration of oxygen and iron ions may be enhanced in the presence of fluid phase through the nano-crack and tunnels within

TABLE 3. Fractional coordinates of atoms and vacancies (Vac) in laihunite-1M, laihunite-2M, and laihunite-3Or structures based on fayalite setting (see CIF¹)

Atom	x	y	z	Atom	x	y	z
Laihunite-1M							
Space group $P2_1/b$, $\alpha = 91.39^\circ$, $\beta = 90^\circ$, $\gamma = 90^\circ$							
Fe1	0.00000	0.00000	0.00000	Fe2	0.50625	0.22833	0.25940
Si1	0.56010	0.09479	0.74789	Vac	0.00000	0.00000	0.50000
O1	0.22426	0.10578	0.76075	O2	0.32784	0.05564	0.24005
O3	0.70433	0.17868	0.53945	O4	0.72661	0.17100	0.96877
Laihunite-2M							
Space group $P2_1/b$, $\alpha = 90.79^\circ$, $\beta = 90^\circ$, $\gamma = 90^\circ$							
Fe1A	0.00000	0.00000	0.50000	Fe1B	0.50331	0.49330	0.23409
Fe2A	0.01657	0.72036	0.37275	Fe2B	0.50465	0.77065	0.11864
Vac	0.00000	0.00000	0.00000				
Si1	0.57023	0.90246	0.37007	Si2	0.06434	0.59508	0.11892
O1	0.23210	0.90769	0.37049	O2	0.76982	0.10599	0.12715
O3	0.17407	0.44476	0.12487	O4	0.78700	0.54831	0.37052
O5	0.29257	0.17861	0.01647	O6	0.71221	0.83176	0.47971
O7	0.23020	0.66883	0.22619	O8	0.78605	0.32914	0.25917
Laihunite-3Or							
Space group $Pbnm$, $\alpha = 90^\circ$, $\beta = 90^\circ$, $\gamma = 90^\circ$							
Fe2A	0.50432	0.22994	0.08029	Fe2B	0.01683	0.28260	0.25000
Fe1A	0.99655	0.00782	0.15910	Vac	0.00000	0.00000	0.00000
Si1	0.56779	0.10031	0.25000	Si2	0.43560	0.90602	0.08000
O1	0.22939	0.09520	0.25000	O2	0.73010	0.39511	0.08605
O3	0.17528	0.55647	0.08450	O4	0.20721	0.32165	0.01079
O5	0.22973	0.33279	0.15182	O6	0.71193	0.17355	0.17585
O7	0.28912	0.04515	0.75000				

TABLE 4. Structural data of Fe-O octahedra in fayalite, laihunite-1M, laihunite-2M, and laihunite-3Or

	Fayalite	1M	2M	3Or		
M1-O (Å)	2.16	2.15	2.16	2.16	2.16	
Volume of octahedra (Å ³)	12.79	12.38	12.59	12.79	12.58	
Bond length variation	± 0.02	± 0.02	± 0.03	± 0.02	± 0.02	
M2-O (Å)	2.17(Fe ²⁺)	2.04(Fe ³⁺)	2.04(Fe ³⁺)	2.16(Fe ²⁺)	2.04(Fe ³⁺)	2.16(Fe ²⁺)
Volume of octahedra (Å ³)	13.02	10.90	10.89	12.91	10.89	12.90
Bond length variation	± 0.04	± 0.03	± 0.02	± 0.04	± 0.03	± 0.04

Note: Structure of fayalite is from Fujino et al. (1981).

TABLE 5. Difference between Si and Fe in their z coordinates among proposed models of 1-layer laihunite and fayalite

Authors	Si	Fe2	difference
Fayalite by Fujino et al. (1981)	0.25	0.25	0
Ferrifayalite Group (1976)	0.2220	0.2730	0.0510
Fu et al. (1982)	0.2430	0.2740	0.0310
Tamada et al. (1983)	0.2491	0.2579	0.0088
Chatterjee and Saha-Dasgupta (2010)	0.2501	0.2596	0.0095
This study	0.2521	0.2594	0.0073

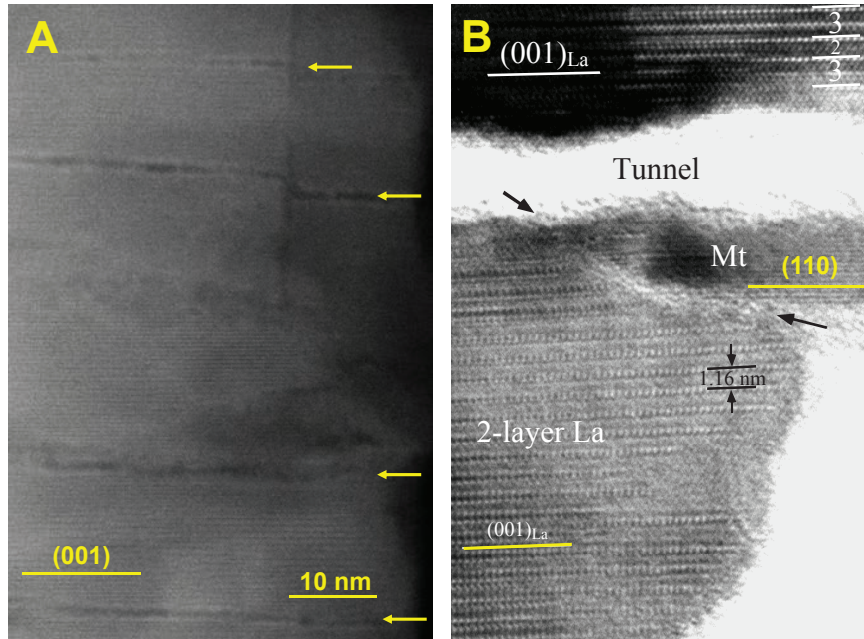


FIGURE 12. (a) A low-magnification Z-contrast image showing nano-tunnels or nano-cracks (indicated by arrows) in the laihunite. (b) A HRTEM image showing a magnetite nano-precipitate in a nano-tunnel.

the crystal (Fig. 12). Magnetite nano-precipitates occur at some nano-tunnels. Observed epitaxial relationship between the magnetite precipitates and laihunite host is one of magnetite $\{111\} \sim // \{100\}$ of laihunite, and one of magnetite $\{110\} \sim // (001)$ of laihunite.

IMPLICATIONS

It is very challenging to solve crystal structures of nano-precipitates in host minerals using X-ray diffraction and TEM.

Our results provide a new way for solving the crystal structures of nano-crystals in or intergrown with host minerals, and locally ordered domains in interstratified clay minerals. Z-contrast imaging can provide information about topology of the crystal structure, and DFT calculation provides accurate coordinates of the atoms within a unit cell. The observed vacancy ordering in Fe-rich olivine may provide information about highly anisotropic diffusion of atoms in Fe³⁺-bearing olivine crystals. Vacancy

layers in Fe³⁺-bearing olivine may behave as a “highway” for atom diffusion. Z-contrast imaging is a powerful tool for direct observation of vacancies and other defects. The method can be used for studying oxidation of iron and vacancy ordering in other minerals, such as Fe-bearing olivine minerals, and chain silicate minerals, and Fe-bearing oxide minerals. The combination of complementary methods described in this paper can be used for observing and quantifying local ordering of Fe atoms and vacancies in partially oxidized Mg-rich olivine crystals reported by Janney and Banfield (1998) and Konishi and Xu (2012).

ACKNOWLEDGMENTS

This work is supported by NASA Astrobiology Institute (N07-5489) and NSF (EAR-095800). Authors thank Alex Kivit for optimizing instrument condition. Author also thank Major Research Instrumentation (MRI) program of NSF for funding the aberration corrected STEM. Xu thanks David Veblen for supporting his early TEM works at Johns Hopkins University. Xu and Fu acknowledge K. C. Wong Education Foundation (Hong Kong) for supporting early stage of this collaborative research.

REFERENCES CITED

- Banfield, J.F., and Bailey, S.W. (1996) Formation of regularly interstratified serpentine-chlorite minerals by tetrahedral inversion in long-period serpentine polytypes. *American Mineralogist*, 81, 79–81.
- Banfield, J.F., Veblen, D.R., and Jones, B.F. (1990) Transmission electron microscopy of subsolidus oxidation and weathering of olivine. *Contributions to Mineralogy and Petrology*, 106, 110–123.
- Banfield, J.F., Dyar, M.D., and McGuire, A.V. (1992) The defect microstructure of oxidized mantle olivine from Dish Hill, California. *American Mineralogist*, 77, 977–986.
- Chatterjee, S., and Saha-Dasgupta, T. (2010) First-principles simulations of structural, electronic, and magnetic properties of vacancy-bearing Fe silicates. *Physical Review*, 81, 155105.
- Chou, B.S. (1985) Fine textures in silicate minerals. In K.H. Kuo and H.Q. Ye, Eds., *High-resolution Electron Microscopy*, p. 423–445. Science Press, Beijing (in Chinese).
- Cococcioni, M., Corso, A.D., and de Gironcoli, S. (2003) Structural, electronic, and magnetic properties of Fe₂SiO₄ fayalite: Comparison of LDA and GGA results. *Physical Review*, 67, 094106.
- Dudarev, S.L., Botton, G.A., Savrasov, S.Y., Humphreys, C.J., and Sutton, A.P. (1998) Electron-energy-loss spectra and the structural stability of nickel oxide: An LSDA+U study. *Physical Review*, 57, 1505–1509.
- Ferrifayalite Research Group (1976) Ferrifayalite and its crystal structure. Department of Geology of Peking University and Institute of Geology and Mineral Resources of Chinese Academy of Geological Sciences. *Acta Geologica Sinica*, 2, 161–175 (in Chinese).
- Fu, P., Kong, Y., and Zhang, L. (1982) Domain twinning of laihunite and refinement of its crystal structure. *Chinese Journal of Geochemistry*, 1, 115–133.
- Fujino, K., Sasaki, S., Takeuchi, Y., and Sadanaga, R. (1981) X-ray determination of electron distributions in forsterite, fayalite and tephroite. *Acta Crystallographica*, 37, 513–518.
- Janney, D.E., and Banfield, J.F. (1998) Distribution of cations and vacancies and the structure of defects in oxidized intermediate olivine by atomic-resolution TEM and image simulation. *American Mineralogist*, 83, 799–810.
- Kirkland, E.J. (1998) *Advanced Computing in Electron Microscopy*. Plenum Press, New York, 250 pp.
- Kitamura, M., Shen, B., Banno, S., and Morimoto, N. (1984) Fine texture of laihunite, a nonstoichiometric distorted olivine-type minerals. *American Mineralogist*, 69, 154–160.
- Kondoh, S., Kitamura, M., and Morimoto, N. (1985) Synthetic laihunite (□_xFe_{2-3x}Fe_{3x}SiO₄), an oxidation product of olivine. *American Mineralogist*, 70, 737–746.
- Konishi, H., and Xu, H. (2012) Direct observation of vacancies and iron atoms in a Mg-rich olivine using Z-contrast imaging. *Microscopy and Microanalysis*, 18, Supplement S, 2, 348–349.
- Kresse, G., and Furthmüller, J. (1996) Efficiency of ab-initio total energy calculations for metals and semiconductors using a plane-wave basis set. *Computational Materials Science*, 1, 15–50.
- Laihunite Research Group (1976) Laihunite—a new iron silicate mineral. *Geochimica*, 2, 95–103 (in Chinese).
- Li, H., Liu, W., Kong, Y., and Fu, P. (1981) The lattice fringes of laihunite. *Kexue Tongbao*, 10, 590–592 (in Chinese).
- Livi, K.J.T., and Veblen, D.R. (1987) “Eastonite” from Easton, Pennsylvania: A mixture of phlogopite and a new form of serpentine. *American Mineralogist*, 72, 113–125.
- Noguchi, T., Nakamura, T., Misawa, K., Imae, N., Aoki, T., and Toh, S. (2009) Laihunite and jarosite in the Yamato 00 nakhlites: alteration products on Mars? *Journal of Geophysical Research*, 114, E10004, doi:10.1029/2009JE003364.
- Pennycook, S. (2002) Structure determination through Z-contrast microscopy. In P.W. Hawkes, P.G. Merli, G. Calestani, and M. Vittori-Antisari, Eds., *Advances in Imaging and Electron Physics*, 123, p. 173–206. Elsevier, Amsterdam.
- Perdew, J.P., Burke, K., and Ernzerhof, M. (1996) Generalized gradient approximation made simple. *Physical Review Letters*, 18, 3865–3868.
- Putnis, A. (1979) Electron petrography of high-temperature oxidation in olivine from Rhum layered intrusion. *Mineralogical Magazine*, 43, 293–296.
- Schaefer, M.W. (1983) Measurements of iron (III)-rich fayalites. *Nature*, 303, 325–327.
- (1985) Site occupancy and two-phase character of “fayalite”. *American Mineralogist*, 70, 729–736.
- Shen, B., Tamada, O., Kitamura, M., and Morimoto, N. (1982) The superstructure of laihunite (Fe₂³⁺Fe₁₀²⁺SiO₄). *Scientia Geologica Sinica*, 3, 341–342 (in Chinese).
- (1984) Superstructure of laihunite-3M (□_{0.4}Fe_{0.8}³⁺Fe_{0.8}²⁺SiO₄). *American Mineralogist*, 71, 1455–1460.
- Shi, F. (2013) *Advanced electron microscopy of novel ferromagnetic materials and ferromagnet/oxide interfaces in magnetic tunnel junctions*. Ph.D. Dissertation, University of Wisconsin-Madison.
- Stackhouse, S., Stixrude, L., and Karki, B.B. (2010) Determination of the high-pressure properties of fayalite from first-principles calculations. *Earth and Planetary Science Letters*, 289, 449–456.
- Sueno, S., Matsuura, S., and Prewitt, C.T. (1985) Fe-deficient olivine structure type minerals from Colorado, U.S.A. and Japan. *Mineralogical Journal (Japan)* 12, 376–392.
- Tamada, O., Shen, B., and Morimoto, N. (1983) The crystal structure of laihunite (□_{0.4}Fe_{0.8}³⁺Fe_{0.8}²⁺SiO₄). *Mineralogical Journal*, 11, 382–391.
- Wang, S. (1982) The stability of laihunite—A thermodynamic analysis. *Chinese Journal of Geochemistry*, 1, 233–243.
- Xu, H., and Veblen, D.R. (1996) Interstratification and other reaction microstructures in the chlorite-berthierine series. *Contributions to Mineralogy and Petrology*, 124, 291–301.
- Xu, H.F., Xu, H.W., and Luo, G. (1992) Domain structures in minerals. *Science in China 35B*: 1218–1223 with plates I and II.

MANUSCRIPT RECEIVED JULY 26, 2013
 MANUSCRIPT ACCEPTED JANUARY 8, 2014
 MANUSCRIPT HANDLED BY HONGWU XU